Predictive Thermodynamic Model for Solvent Extraction of Iron(III) by Tri-*n*-butyl phosphate (TBP) from Chloride Media

Rayco Lommelen,[a*] Brecht Dewulf[a], Jakob Bussé[a] and Koen Binnemans[a]

[a]KU Leuven, Department of Chemistry, Celestijnenlaan 200F, P.O. box 2404, B-3001 Leuven, Belgium

* Corresponding author: Email: rayco.lommelen@kuleuven.be; Phone: +32 16 37 47 82

ABSTRACT

Hydrometallurgical processes are crucial to reducing the environmental impact of metal recovery, yet dealing with iron impurities is a major challenge. This paper presents a semi-empirical predictive thermodynamic model for iron removal from chloride media by solvent extraction with tri-*n*-butyl phosphate (TBP). This model is built upon the OLI mixed-solvent electrolyte framework (OLI-MSE). It goes beyond traditional thermodynamic models by incorporating the non-ideality of both the aqueous and organic phases in a single, chemistry-based thermodynamic model. On top of the OLI-MSE framework lies the chemical model that depicts the extraction of Fe(III) by forming an ion pair between the $FeCl_4^-$ anions and protonated TBP ($TBPH^+$) molecules in the organic phase. The iron(III)-containing ion pair in the organic phase is further stabilized by interactions with neutral TBP molecules. Developing the model required modeling the Fe(III) – chloride chemistry in the aqueous phase, optimizing the HCl extraction model, and fitting the parameters between $FeCl_4^-$, $TBPH^+$, and TBP to experimental solvent extraction data. The resulting thermodynamic model can predict the solvent extraction of iron(III) from complex feed solutions by TBP in aliphatic diluents at all concentrations up to undiluted TBP. It can be used to calculate the equilibrium energies and composition, and the species present at equilibrium.

KEYWORDS: chemical thermodynamics; iron; liquid-liquid equilibria; mixed-solvent electrolyte model; solvent extraction

1. INTRODUCTION

Efficient removal of iron impurities is one of the main challenges in the development of hydrometallurgical flowsheets [1,2]. The presence of iron in the pregnant leach solution (PLS) can lead to undesirable precipitation of insoluble compounds, resulting in contamination of the final product, and consumption of an excess of reagents. Furthermore, the iron recovery and conversion to saleable products can improve the economics of the whole process and reduce the amount of waste [3]. Hence, iron removal has become a critical aspect of metallurgical processing routes.

Typically, precipitation is used to remove iron from the PLS in hydrometallurgical processes [4–7]. The pH must be increased after acidic leaching to precipitate iron(III) as a hydroxide. This leads to the consumption of large amounts of base, a significant loss of acid, and increased waste production. Thus, the removal of iron could benefit from a more circular approach [2]. Solvent extraction of iron by a solvating extractant seems a viable alternative that mitigates these problems [8]. Herein, the extractant facilitates the transfer of iron from an aqueous to the organic phase, preferably without co-extraction of other elements. This technique requires the complexation of Fe(III) with anionic ligands to form extractable iron complexes.

A well-known example is the extraction of Fe(III) from chloride media by tri-*n*-butyl phosphate (TBP) [9,10]. TBP is a cheap and frequently used extractant that allows the extraction of metal-chloride complexes. It is quite selective for Fe(III) over many other metals and it allows for easy stripping of extracted Fe(III) by using water. Sulfate media are unsuitable for extraction by TBP because sulfate does not form Fe(III) sulfato complexes that can be extracted by TBP or other solvating extractants [11]. Also, investigating Fe(II) extraction by TBP is of limited relevance because Fe(II) is not extracted to a significant extent by TBP [12].

A predictive thermodynamic model could benefit the development of unit operations for solvent extraction of Fe(III) by TBP in new flowsheets, and the optimization of the extraction conditions in an existing process. Iron removal through solvent extraction involves a complex interplay between many chemical species distributed over two liquid phases. The distribution of Fe(III) between the aqueous and organic phases must be well understood, considering variables like pH, temperature, ligand concentrations, and phase ratios. In addition to providing insights into these complex equilibria, thermodynamic modeling helps to predict how process variables will affect Fe(III) extraction efficiency, allowing for the creation and optimization of effective solvent extraction circuits.

Currently available thermodynamic models for the solvent extraction of metals have limited predictability. They do not perform well when used to predict solvent extraction equilibria outside the range of conditions used to build the model [13]. The simplest models, e.g. Isocalc^{TM} of BASF and MINCHEM of Solvay (now Syensqo), are purely empirical [14–16]. Some chemical information is introduced by considering equilibrium constants of chemical reactions, but still using concentrations instead of activities [17,18]. Supramolecular interactions should be considered to account for deviations from thermodynamic ideal behavior. Activity equations can represent these interactions to convert concentrations to activities. Even when non-ideality in the aqueous phase is incorporated into the model, a purely empirical expression for the extraction equilibrium constant is still required when neglecting the organic phase non-ideality [19–22]. Baes developed a solvent extraction model (SXFIT) that considers the non-ideality of both the aqueous and organic phases, but their model still uses two separate thermodynamic frameworks to describe both phases while the nature of chemical interactions is indifferent to the phase [23]. SXFIT could also calculate volume changes, based on solution densities. Another approach is to include

additional metal-extractant species in the model to account for the remaining variability in the extraction behavior. These species are often purely hypothetical since there is no experimental evidence of their existence. Hence, the resulting model may be chemically inaccurate when no conclusive experimental evidence of such species is presented.

A predictive thermodynamic model should account for the non-ideality, or intermolecular interactions, in both the aqueous and organic phases, while using a single thermodynamic framework. This is even more important when predicting the equilibrium composition of the system for conditions relevant to the hydrometallurgical industry (concentrated, multi-element solutions). These conditions, and the search for cost-efficient processes lead to high metal loadings of the organic phase. The increased ionic structure of the organic phase, along with significant amounts of coextracted water, emphasizes the need to integrate the non-ideal behavior of the organic phase into a model capable of accurately predicting the equilibrium in industrially relevant solvent extraction processes [24].

The most rigorous and accurate modeling of the non-ideal behavior of the organic phase requires statistical thermodynamics [25–30]. In principle, all the thermodynamic properties can be calculated from the intermolecular forces in this way. However, there are formidable challenges. Not only is the exact nature of these forces usually unknown, but even given such knowledge, an accurate calculation of the properties is practically impossible. So, while statistical thermodynamics is intellectually attractive and some useful results are already available, it is unrealistic to believe that process-design engineers and plant operators could apply statistical thermodynamics to optimize complex SX processes.

Thus, a compromise can be made by using one single semi-empirical activity model [31]. The equations in this model should be founded in physical chemistry, but they also require adjustable

interaction parameters that must be optimized by fitting these equations to experimental data. These interaction parameters typically contain the interaction energy between two or more species, but they cannot be calculated from first principles due to the necessity of introducing assumptions in the activity equations to manage the complexity of mixed-solvent electrolyte systems.

Our previous research has shown that the Mixed-solvent Electrolyte (MSE) framework as implemented in the software of OLI Systems can be used to model the solvent extraction of acids [32–34]. OLI Systems corroborated the feasibility of creating a solvent extraction model for rare earth extraction by 2-ethylhexyl phosphonic acid (HEHEHP) based on the OLI-MSE framework, although they appear to underutilize the framework [35]. This model still incorporates numerous (possibly fictitious) extractant and metal-extractant species, and it is not built with data representing high metal loading in the organic phase. This high metal loading will cause significant deviations from ideality in the organic phase, and it is important to take into account these effects when one wants to utilize a solvent extraction model on an industrial scale. Nevertheless, this work shows that OLI-MSE-based solvent extraction models can be integrated into flowsheet simulators to build multi-stage, continuous, counter-current solvent extraction processes.

In this paper, we present a thermodynamic model based on the OLI-MSE framework that can predict the solvent extraction equilibria of the Fe(III) – chloride – TBP system with *n*-dodecane as model diluent and hydrochloric acid as the main chloride source up to high metal loading. To this end, we modeled the aqueous phase chemistry of Fe(III) in chloride media, and we investigated the extraction mechanism of Fe(III). Next, data on the Fe(III) – chloride – TBP system were collected to fit the interaction parameters using the semi-empirical equations of the OLI-MSE framework. The model was finally validated by considering solvent extraction data not used to build the model.

2. EXPERIMENTAL

2.1. Chemicals

Nitric acid (65 wt%) was purchased from VWR (Leuven, Belgium). Hydrochloric acid (~37 wt%) and *n*-dodecane (99%) were purchased from Fisher Scientific (Geel, Belgium) The aqueous iron and scandium standards (1000 mg L^{-1} in 2–5% HNO_3) and tri-*n*-butyl phosphate (TBP) (>99%) were obtained from Chem Lab (Zedelgem, Belgium). $FeCl_3$ (>98.5%) was purchased from Carl Roth (Belgium). Water was always of ultrapure quality, deionized to a conductivity of less than 0.055 µS cm^{-1} (298.15 K) with a Merck Millipore Milli-Q Reference A+ system. All chemicals were used as received, without any further purification.

2.1. Solvent extraction experiments

Two aqueous Fe(III) solutions were prepared by dissolving anhydrous $FeCl_3$ in 1.0 and 3.0 mol L^{-1} HCl solution. Aliquots (5 mL) of these aqueous solutions were contacted with 50 or 100 vol% TBP (5 mL) in 20 mL glass vials. These vials were placed in aluminum blocks on magnetic stirrers/heaters to stir the solution for 30 min at 600 rpm at a controlled temperature between 25 and 65 °C. After the stirring was stopped, the two phases were allowed to disengage gravitationally at the controlled temperature. Then, the aqueous and organic phases were physically separated while the vials remained in the heating block.

The metal concentrations in the aqueous phase and starting solutions were determined by inductively coupled plasma optical emission spectroscopy (ICP-OES) using a PerkinElmer Avio 500 spectrometer. This spectrometer was equipped with an axial/radial dual plasma view, a GemCone High Solids nebulizer, a baffled cyclonic spray chamber, and a demountable quartz

torch featuring a 2.0 mm internal diameter alumina injector. For sample, calibration solution, and quality control solution preparation, all solutions were diluted with HNO_3 (2 vol%). All ICP-OES spectra were measured in triplicate. The error on the triplicate measurements was less than 5%. As this error only minimally affected the results, error bars were omitted from the graphs to enhance readability.

Calibration curves were created using solutions with iron concentrations of 0.05, 0.1, 1, 5, and 10 mg L^{-1}, which were prepared from a standard solution. To verify the instrument's performance, quality checks were conducted using 5 mg L^{-1} metal solutions. Scandium (5 mg L^{-1}) was added to all samples, calibration solutions, and quality controls and utilized as an internal standard.

The iron concentration in the organic phase was determined by a mass balance approach, accounting for any volume changes. These volume changes were predicted using OLI-MSE calculations based on the acid-TPB SX model that was built with mass-balance and organic density data [32]. No precipitation or third-phase formation occurred during the period between the experiments and the measurements.

Extraction of HCl was determined via an automated argentometric titration using a Mettler-Toledo DMi141-SC combined silver ring electrode, a Mettler-Toledo titrator T5 Excellence, and an InMotion Flex autosampler. The aqueous phases and starting solutions (between 20 and 500 µL) were mixed with 2 mL of Triton^{TM} X-100 (5 wt%) in 30 mL of Milli Q water. Then, the pH was raised to 4–4.5 by the addition of 0.1 mol L^{-1} KOH using a Mettler-Toledo DMi111-SC-combined glass pH electrode. These diluted solutions were titrated with a calibrated solution of $AgNO_3$ (0.05 mol L^{-1}).

To determine the HCl concentration in the organic phase, first, the HCl acid concentration in the aqueous phase was calculated based on the chloride titration results. The argentometric titration measures the total chloride concentration, including that of $FeCl_3$. To account for the chlorides from Fe(III), three times the initial Fe(III) concentration determined by ICP-OES was subtracted from the total chloride concentration in the starting solutions (equation (1)). Equation (1) was also used to determine the HCl concentration in the aqueous phase at equilibrium, but now using the equilibrium aqueous Fe(III) concentration. Subsequently, the organic HCl content was calculated using the mass balance. For this, the aqueous and organic phase volume changes were calculated in OLI using the acid-TPB SX model [32].

$$[\mathrm{HCl}] = [\mathrm{Cl^-}]_{\mathrm{total}} - 3[\mathrm{Fe(III)}] \quad (1)$$

3. MODEL DESCRIPTION

3.1. Thermodynamic framework

The Mixed-Solvent Electrolyte (MSE) framework version 11.5 from OLI Systems Inc. (Parsippany NJ) was utilized to build the thermodynamic model on Fe(III) extraction by TBP from chloride media. The software packages OLI Studio 11.5, OLI Databook 11.5, and OLI Chemistry Wizard 11.5 of OLI Systems Inc. (Parsippany NJ) were used.

Within the OLI-MSE thermodynamic framework, both electrolytes and non-electrolytes can be described in mixed-solvent systems, which involve combinations of aqueous and organic solvents [33,34]. As a result, this framework is well-suited for computing liquid-liquid equilibrium (LLE) data, which is essential for describing the solvent extraction process of Fe(III) from chloride media by TBP. The OLI-MSE framework accomplishes this by merging speciation-based standard-state thermodynamic properties, such as the standard-state Gibbs free energy (G^0), with complex activity-coefficient equations that consider the physical interactions between molecules. The excess Gibbs free energy (G^{EX}) is employed in the activity equations:

$$\frac{G^{EX}}{RT} = \frac{G_{SR}^{EX}}{RT} + \frac{G_{MR}^{EX}}{RT} + \frac{G_{LR}^{EX}}{RT} \quad (2)$$

This G^{EX} is further divided into three components: short-range (*SR*), mid-range (*MR*), and long-range (*LR*) contributions, where *R* represents the universal gas constant and *T* denotes the absolute temperature in Kelvin. The SR and MR contributions require binary interaction parameters that represent the interaction energy between two species. To find the values for these interaction parameters, the OLI-MSE activity equations should be fitted to experimental data. For solvent extractions, these are typically data on the distribution or concentration of the relevant species.

The concentration in the organic phase and Gibbs free energy of transfer $\Delta G_{TR}(\mathrm{A})$, equation (3) of a certain species or a collection of species (*A*) is used in the present work.

$$\Delta G_{TR}(\mathrm{A}) = -RT \cdot ln(D(\mathrm{A})) \quad (3)$$

Where *D(*A*)* is the distribution ratio of A, which is the ratio of the concentration of A in the organic and the aqueous phases. The $\Delta G_{TR}(\mathrm{A})$ was chosen because it closely represents the thermodynamics of a solvent extraction as present in the OLI-MSE framework. Also, water activity, Fe(III) speciation, and HCl extraction data are used to find the most physicochemically accurate interaction parameters.

Furthermore, the density of the aqueous and organic phases are calculated by the OLI-MSE framework to accurately convert the mole fraction or molality-based scales of the thermodynamic system to the more frequently used molarity or mass-per-volume-based scales in hydrometallurgy. These densities are accurately calculated by assigning molar volumes to all relevant chemical species, adding density interaction parameters to certain combinations of species, and calculating the full composition of a phase [33]. The calculation of both the density and the full composition of every phase allows to predict volume changes during solvent extraction. A more detailed description of the OLI-MSE framework concerning solvent extraction can be found in our previous publication [32].

3.2. Chemical model

The extraction of Fe(III) from acidic chloride media by TBP is accompanied by the extraction of HCl. Hence, both the extraction of HCl and Fe(III) should be calculated to simulate the complete

equilibrium. Therefore, the Fe(III) extraction model presented below is built upon our thermodynamic model for the extraction of mineral acids by TBP [32]. That model incorporates a universal extraction mechanism for mineral acids. Strong acids, like HCl, protonate TBP upon extraction to form $TBPH^{+}\cdot Cl^{-}$, while weaker acids, like H_3PO_4, do not protonate TBP and they are simply solvated by TBP in the organic phase.

In both the acid – TBP and the Fe(III) – chloride – TBP thermodynamic models, *n*-dodecane was selected as the diluent. *n*-Dodecane can approximate a wide range of aliphatic diluents, including kerosene. Moreover, it is suitable for integration into a thermodynamic model because only interaction parameters with one well-defined compound are required, as opposed to the complex task of defining and optimizing numerous interaction parameters for the mixture of compounds found in kerosene.

TBP is a solvating extractant (or neutral extractant), which generally extracts metal ions as neutral complexes (equation (4)) [36,37]. The positive charge of the metal ions is neutralized by complexation with the right number of anions. A number of TBP molecules coordinate with their phosphoryl oxygen atoms to this neutral metal complex to saturate the first coordinating sphere of this metal complex. This water-insoluble structure resides in the organic phase, completing the extraction of the metal ion. Some authors invoke this mechanism for the extraction of Fe(III) by TBP (equation (4)) to form $FeCl_3(TBP)_3$, although often in combination with other extraction mechanisms [38,39].

$$Fe^{3+} + 3Cl^{-} + 3\overline{TBP} \rightleftharpoons \overline{FeCl_3(TBP)_3} \qquad (4)$$

In aqueous media, one or three water molecules are coordinated to the $FeCl_3$ in the first coordination sphere of iron(III) to obtain a tetrahedral or octahedral geometry [40]. These water

molecules are replaced by TBP upon extraction, which entails an unfavorable dehydration energy. Coordinating one more chloride leads to the formation of tetrahedral $FeCl_4^-$ in aqueous media [40]. This complex does not contain water in its first coordination sphere, avoiding the unfavorable dehydration when $FeCl_4^-$ is extracted by TBP. This results in a frequently published second extraction mechanism: the extraction of $HFeCl_4$ by TBP or $FeCl_4^-$ by $TBPH^+$ [9,38,39,41–43]. Slope analysis suggests that a second TBP molecule participates in this extraction process, resulting in the following overall extraction mechanism:

$$Fe^{3+} + 4Cl^- + H^+ + 2\overline{TBP} \rightleftharpoons \overline{FeCl_4^- \cdot TBPH^+ \cdot TBP} \quad (5)$$

The acid dependence of the Fe(III) extraction becomes evident when performing an experiment at constant chloride concentration and increasing acid concentration [8]. Infrared (IR) absorption spectra of the TBP phase recorded by Hui Su *et al.* suggest that the proton involved in the extraction mechanism is bonded to the phosphoryl oxygen atom [44]. They attributed the peak at 1281 cm^{-1} to the P=O bond of pure TBP. This peak shifts to lower wavenumbers when TBP is loaded with Fe(III) and LiCl, and it shifts further when HCl is used instead of TBP. Furthermore, the shift to lower wavenumbers increases with increasing HCl content in the Fe(III) – TBP phase. This shift to lower wavenumbers indicates a weakening of the P=O bond due to the interaction of a cationic species (e.g. H^+) with the electron-rich oxygen. The $TBPH^+$ and any additional TBP molecules should then stabilize $FeCl_4^-$ in the organic phase. This stabilization most likely occurs in the second coordination sphere, as $FeCl_4^-$ is already coordinatively saturated [40].

Thus, our thermodynamic model should at least reproduce the acid-dependent extraction mechanism shown in equation (5). In order to obtain a thermodynamic model with predictive power, the introduction of too many chemical species should be avoided. With this in mind, Fe(III)

was extracted in the model as $FeCl_4^-$ by introducing attractive interaction energies between $FeCl_4^-$ and $TBPH^+$/TBP. This represents the formation of the ion pair as shown in equation (5). No specific Fe(III)–TBP complexes were required in the thermodynamic model to accurately reproduce the available extraction data.

4. RESULTS AND DISCUSSION

4.1. Aqueous Fe(III) chemistry

The complexation behavior of Fe(III) in the aqueous phase is of vital importance for its extraction by a solvating extractant like TBP. This involves the coordination of up to four chloride anions with increasing chloride concentration, while the public OLI-MSE database (version 11.5) as supplied by OLI Systems contains only the Fe^{3+}, $FeCl^{2+}$, and $FeCl_2^{+}$ species [40]. As a result, the first task towards creating the Fe(III) – chloride – TBP thermodynamic model was the expansion of the aqueous Fe(III) – chloride chemistry to cover all experimentally observed Fe(III) – chloride species.

First, standard state thermodynamic properties for the Fe(III) – chloride species were estimated. The standard state Gibbs free energy of formation (ΔG_f^0) of the species was calculated using the equilibrium constants reported by Liu *et al*. and $\Delta G_f^0(Fe^{3+})$ [40]. The standard state entropies (S^0) of the Fe(III) – chloride species were approximated by summing the S^0 of the chloride anions and that of Fe^{3+} for each species. The $\Delta G_f^0(Fe^{3+})$ and $S^0(Fe^{3+})$ were taken from the public OLI-MSE database to obtain a consistent thermodynamic model. The standard-state enthalpy of formation (ΔH_f^0) of the Fe(III) species (X) was then calculated as follows:

$$\Delta H_f^0(\mathrm{X}) = \Delta G_f^0(\mathrm{X}) + T\left(S^0(\mathrm{X}) - \sum_i v_i S^0(i)\right) \tag{6}$$

Where T is the absolute temperature in Kelvin and the summation runs over all elements (i) in their standard state that make up X with stoichiometry v_i.

The final values of these thermodynamic properties, as present in the optimized thermodynamic model, can be found in Table 1. Most values deviate from their initial estimate in order to obtain a better fit between the thermodynamic model and the available experimental data (*vide infra*). Only the values for Fe^{3+} were kept constant during the optimization to maintain consistency with the public OLI-MSE database. The Uniquac size and surface parameters for the short-range contributions of all Fe(III) – chloride species do not require optimization. They are fixed at 0.92 and 1.4, respectively, as is customary for inorganic ions in the OLI software [33].

Table 1. Standard-state properties of the relevant species in the thermodynamic model and their final values after optimization with experimental data.

Species	ΔG_f^0	ΔH_f^0	S^0	**Source**
	kJ mol^{-1}	**kJ mol^{-1}**	**J mol^{-1} K^{-1}**	
Fe^{3+}	-17.25	-118.1	-277.6	General OLI-MSE database
$FeCl^{2+}$	-159.0	-244.5	-97.85	This work
$FeCl_2^+$	-292.8	-388.5	-4.028	This work
$FeCl_3$	-415.5	-519.94	94.97	This work
$FeCl_4^-$	-531.1	-657.6	149.23	This work
TBP	-812.9	-1423	234.7	General OLI-MSE database
$TBPH^+$	-800.1	-1381	266.2 [a]	[32]

[a] updated in this work

The standard-state properties only represent the chemistry of Fe(III) at infinitely dilute conditions [33]. To obtain an accurate model at higher concentrations of Fe(III), HCl, and metal chloride salts, the OLI-MSE framework requires interaction parameters to calculate the activities of all species, instead of their concentrations. The values of these interaction parameters can be found by fitting the activity equations from the OLI-MSE framework to carefully selected experimental data.

Sufficient data on Fe(III) – chloride systems between 25 °C and 90 °C were available in the literature to model all Fe(III) – chloride complexes using the OLI regression module. These data include the speciation of Fe(III) at 25, 60, and 90 °C at varying LiCl concentrations [40], and water activity data from $FeCl_3$ – HCl media [45] and $FeCl_3$ – NaCl systems [46].

Mid-range Fe(III) – H_2O binary interaction parameters were sufficient to accurately fit all the experimental data at room temperature (Figure 1a, Figure 2, and Table 3). These interaction parameters with water represent the changing hydration energy with changing water, chloride, and Fe(III) concentrations. No specific Fe(III) – cation (H_3O^+, Li^+, or Na^+) interaction parameters were required to fit the differences in HCl, LiCl, and NaCl systems. Most likely, H_3O^+, Li^+, or Na^+ ions influence the water activity, which again influences the stability of the Fe(III) species. The public OLI-MSE database already contains the relevant information on HCl, LiCl, and NaCl solutions, as well as that of many other chloride salts. As a result, it is expected that the complexation behavior of Fe(III) is predicted quite accurately in many different chloride systems by OLI using the thermodynamic framework presented here. The speciation changes at 60 and 90 °C were fitted by optimizing the S^0 values of the four Fe(III) – chloride species (Figure 1b and c).

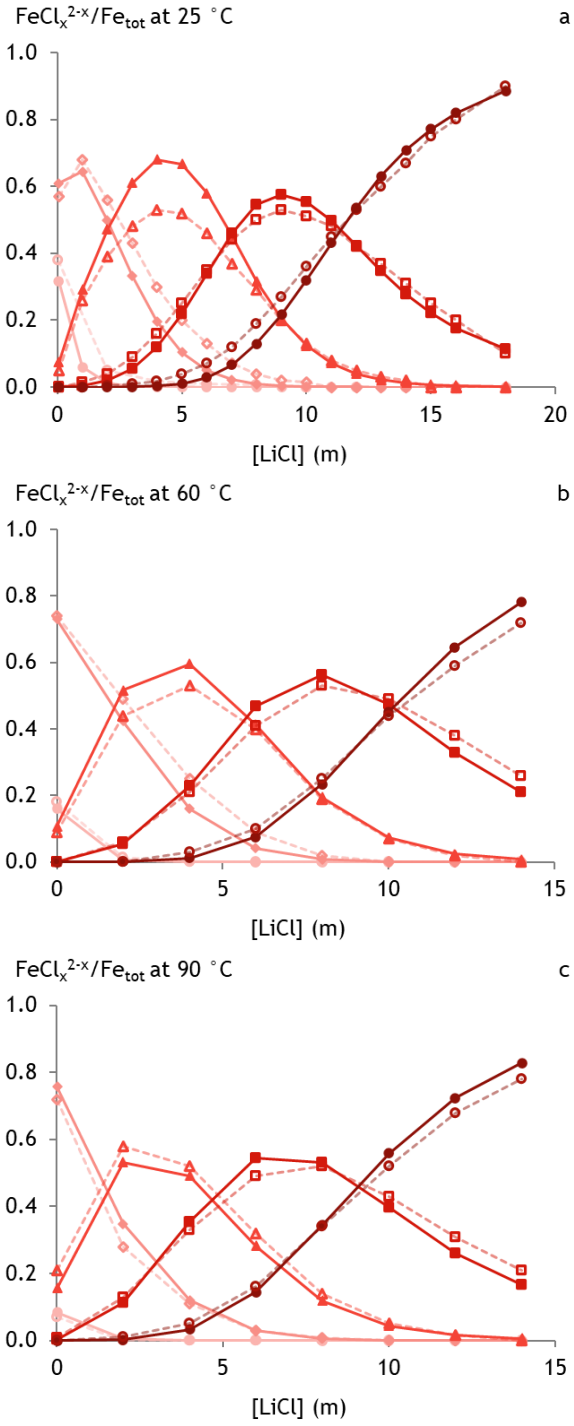

Figure 1. Model fit (filled markers) to the speciation of Fe(III) in LiCl solutions at different temperatures. Experimental data (open markers) originate from Liu et al [40]. Speciation: Fe^{3+} (●), $FeCl^{2+}$ (◆), $FeCl_2^+$ (▲), $FeCl_3$ (■), and $FeCl_4^-$ (●). The total LiCl concentration is given in molality (m).

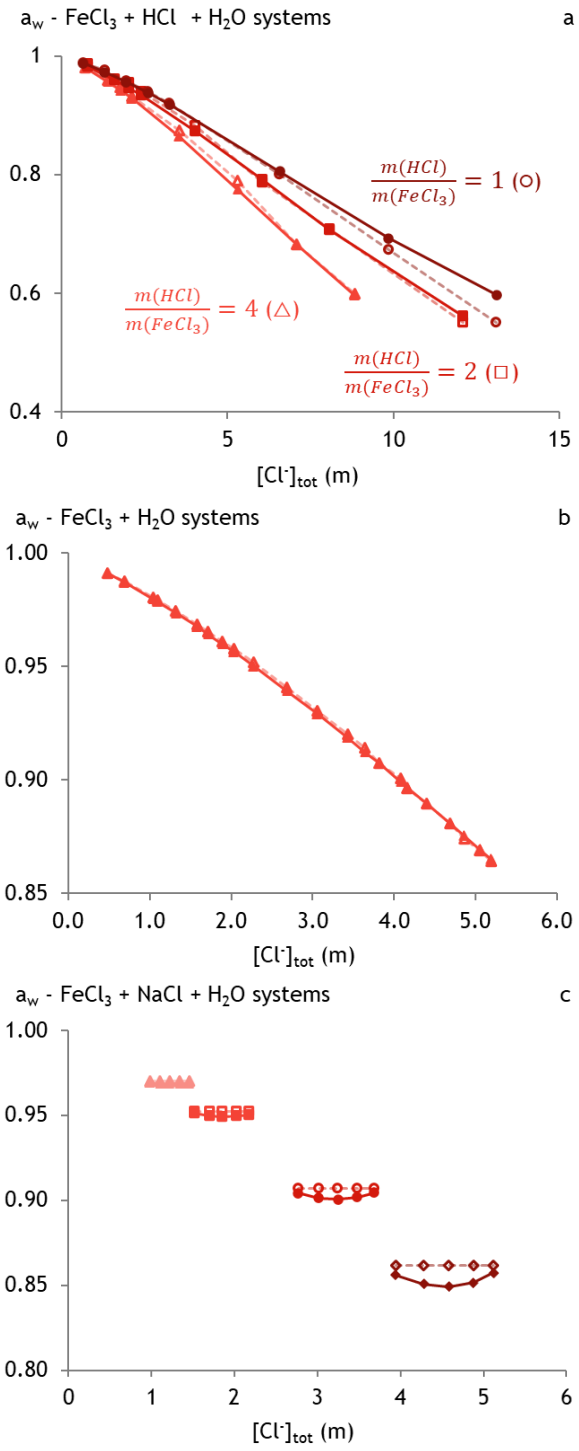

Figure 2. Model fit (filled markers) to water activity (a_w) data at 25 °C. Experimental data (open markers) originate from Awakura et al. (a) and Rumyantsev et al. (b and c) [45,46]. c shows isoactivity data for solutions containing 0.05–1.56 m $FeCl_3$ and 0.09–3.35 m NaCl. m is molality.

By comparing the thermodynamic model with the literature data for the Fe(III) speciation in aqueous LiCl solutions using ordinary least squares (OLS), an appropriate fit was found in which the statistical model explains at least 97.1% of the variation observed within the data (Figure 3, R^2). At 25 °C, there is a statistically significant deviation between the OLS line and the ideal fit line (Figure 3, dotted black line), based on 2 times the standard deviation on the slope of the OLS fit. For the speciation at 60 °C and 90 °C, there is a non-significant difference between the OLS line and the ideal fit line, showing no evidence of a lack of fit between the thermodynamic model and the experimental speciation data. The 95% prediction interval around the mean is an important indicator for the expected error on a prediction by the thermodynamic model on a new experimental measurement. It shows that the predicted mole fraction of a species, in the case of T = 25 °C, can be expected to fall within ± 0.086 (= 8.6%) of the OLS line in 95% of the cases. This prediction interval improves to 0.070 for the speciation at 60 °C and to 0.056 at 90 °C. Both experimental errors and imperfections in the thermodynamic model contribute to this error.

A large part of the error on the OLS analysis originates from the strong correlation between the experimental data for the $FeCl^{2+}$ and the $FeCl_2^+$ species (see Supporting Information). Certainly at 25 °C, the amount of $FeCl_2^+$ is overestimated by the thermodynamic model and that of $FeCl^{2+}$ is underestimated (Figure 3, $FeCl^{2+}$ (◆) and $FeCl_2^+$ (▲)) The *model-free* analysis performed by Liu *et al.* on their UV-VIS spectra of Fe(III) shows negligible differences in the shape of the pure spectra of $FeCl^{2+}$ and $FeCl_2^+$ [40]. They only differ in overall molar absorbance. Given the similar shape of the pure $FeCl^{2+}$ and $FeCl_2^+$ spectra, it is practically impossible to assign correct relative abundances to $FeCl^{2+}$ and $FeCl_2^+$ by the *model-free* analysis of Liu *et al*. Furthermore, the decrease in the prediction error of the thermodynamic model at 60 and 90 °C coincides with a decrease in the difference of the overall molar absorptivity of $FeCl^{2+}$ and $FeCl_2^+$ as calculated by Liu *et* al.

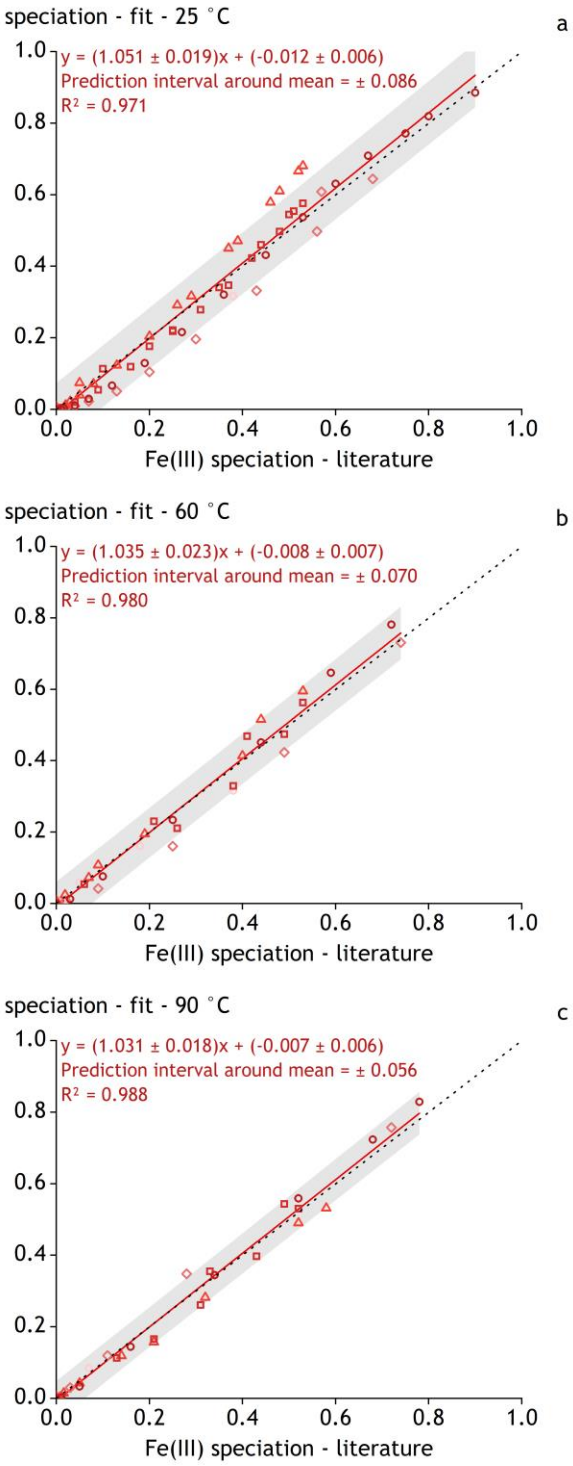

Figure 3. OLS analysis (dark red line) of thermodynamic model fit and experimental Fe(III) speciation data. Data is visually split per species(Fe^{3+} (●), $FeCl^{2+}$ (◆), $FeCl_2^{+}$ (▲), $FeCl_3$ (■), and $FeCl_4^{-}$ (●)), but OLS analysis is performed on the whole dataset per temperature. The graphs also contain perfect fit lines (dotted black), and 95% prediction intervals (light gray).

An OLS analysis of the thermodynamic model fit of experimental a_w data explains 99.4% of the variation observed within the data (Figure 4). The slope of the OLS curve is slightly below one, and the intercept is found somewhat below zero, indicating that the calculated a_w slightly overestimates the experimental observations at lower a_w. At a 95% interval, a predicted a_w value of a new experimental would fall within ± 0.014 (1.4%) of the OLS curve. The ideal fit line (Figure 4, dotted black line) falls within the prediction interval for the experimental a_w range used for the model (0.55 – 1.00). It suggests that there is no significant evidence for a lack of prediction over the whole modeled a_w range.

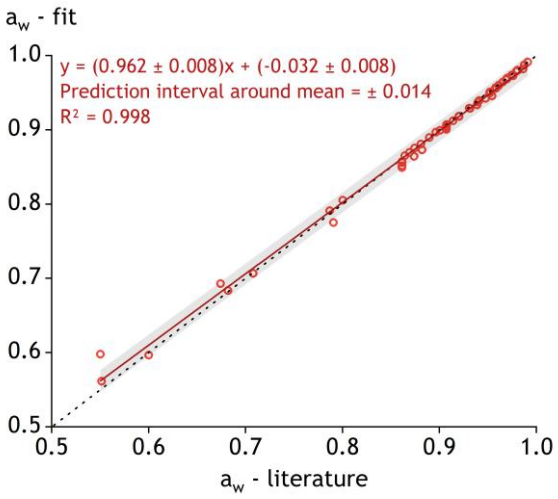

Figure 4. OLS analysis (dark red line) of thermodynamic model fit and experimental Fe(III) water activity (a_w) data. Graph also contains the perfect fit line (dotted black), and 95% prediction interval (light gray).

The relatively low deviation on the fit can be explained partially by the nature of water activity, which is largely determined by the most abundant ions in solutions. In the data used for the model, these are predominantly Cl^-, H_3O^+, and Na^+. The standard and excess thermodynamic data of these ions are already well-defined in the public OLI-MSE database. Nevertheless, significant amounts

of (partially hydrated) Fe(III) and ferrochloride species are present, showing that the influence of the Fe(III) species on the activity of water is also accurately described by the thermodynamic model.

4.2. Update of the HCl extraction model

Thus far, the thermodynamic model contains an accurate description of Fe(III) in aqueous chloride media, and the HCl – TBP – *n*-dodecane chemistry in the organic phase. The thermodynamic data of the latter system are taken from our previous publication [32], but the temperature and extractant concentration dependence of the HCl extraction was slightly optimized to enable more accurate calculations of the extraction of Fe(III) in these systems using recently found literature data. To this end, the binary interaction parameters between HCl/Cl^- and $TBP/TBPH^+$ were refitted using HCl and H_2O extraction data by undiluted TBP from Kertes [47], and Hesford and McKay [48], and with additional experimental data from Hanson and Patel [49]. Eventually, mid-range temperature-dependent binary interaction parameters (equation (7), Table 3) and a reoptimization of $S^0(\mathrm{TBPH^+})$ (Table 1) were used to fit data at different HCl concentrations, TBP concentrations, and temperatures [50].

$$B_{ij}(I_x) = b_{0,ij} + \frac{b_{2,ij}}{T} + \left(c_{0,ij} + \frac{c_{2,ij}}{T}\right) exp\left(-\sqrt{I_x + 0.01}\right) \quad (7)$$

$B_{ij}(I_x)$ represents the ionic-strength-dependent mid-range binary interaction parameters between i and j with I_x the mole-fraction-based ionic strength of the solution. $b_{0,ij}$, $b_{2,ij}$, $c_{0,ij}$, and $c_{2,ij}$ are the individual mid-range binary interaction parameters that reflect the temperature and ionic

strength dependence. To achieve an accurate fit of the HCl extraction at low TBP concentration, mid-range interaction parameters between *n*-dodecane and HCl/Cl^- were also optimized (Table 3).

An OLS analysis was used to analyze the quality of the thermodynamic model fit and experimental data of the HCl extraction by TBP using a plot of the thermodynamic model fitted and experimental $\Delta G_{TR}(\mathrm{HCl})$ values (Figure 5). The OLS analysis was split into one graph for undiluted TBP data and one for the diluted TBP data, because there is a significant difference in the results of the statistical analysis of both systems. Furthermore, the diluted TBP thermodynamic model fit and experimental data were transformed using the natural logarithm (ln) to achieve a constant variance with varying $\Delta G_{TR}(\mathrm{HCl})$. This is common practice when the original data shows significantly more variance on the data points at the extremes of the data interval. As a result, the prediction interval around the mean is expressed in ln(kJ mol^{-1}) for the OLS analysis of the diluted TBP data, and a back transformation is required to obtain the value in kJ mol^{-1}.

There are non-significant deviations between the OLS lines of the data and the ideal fit lines in Figure 5, as the OLS lines fall within 2 standard deviations of the slope (1) and intercept (0) of the ideal fit. Thus, there is no evidence for a lack of fit between the thermodynamic model and the experimental HCl extraction data. At a 95% interval, a predicted $\Delta G_{TR}(\mathrm{HCl})$ by the thermodynamic model will fall within ± 0.696 kJ mol^{-1} of a newly performed experimental value, when this is obtained using undiluted TBP. For diluted TBP, the prediction interval increases to 1.17 kJ mol^{-1}. Note that this deviation can either originate from errors in the thermodynamic model or experimental errors. It is not possible to determine the prediction error on the thermodynamic model alone, based on the fitted data. Therefore, a separate validation of the whole thermodynamic model is performed by predicting other experimental data, focused on the extraction of Fe(III) (*vide infra*).

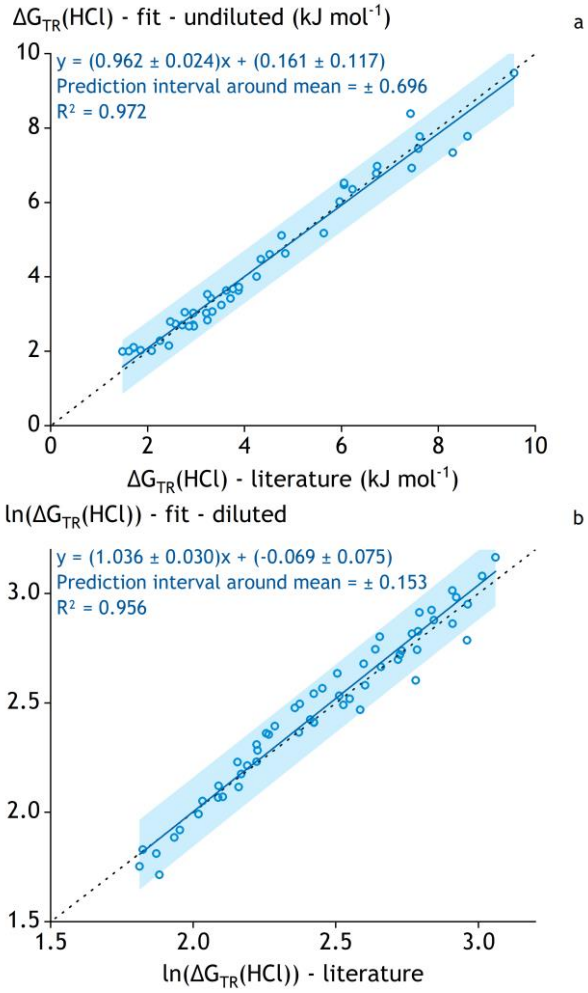

Figure 5. OLS analysis (dark blue lines) of thermodynamic model fit and experimental HCl extraction data of (a) undiluted and (b) diluted TBP. Graphs also show perfect fit lines (dotted black), and 95% prediction intervals (light blue). ln = natural logarithm.

The fitted data include HCl extraction data at 20, 40, 60, and 100 vol% TBP, between 0.01 and 12 mol L^{-1} HCl and at 20, 30 and 50 °C. This covers the useful range of experimental variables for solvent extraction processes of Fe(III) in chloride media. examples of the actual data fits are given in Figure 6. Furthermore, the temperature corrections on the HCl/Cl^- – *n*-dodecane interaction parameters suggest that the diluent also (strongly) influences the temperature dependence of the extraction of HCl, apart from the interaction between HCl/Cl^- and TBP itself.

Note that the reoptimization of $S^0(\mathrm{TBPH}^+)$ also required a slight update of the temperature dependence of the extraction of the other strong acids in the thermodynamic model (HNO_3, H_2SO_4). Weak acids like H_3PO_4 are not affected because $TBPH^+$ is not involved in their extraction. The results of this update can be found in the Supporting Information.

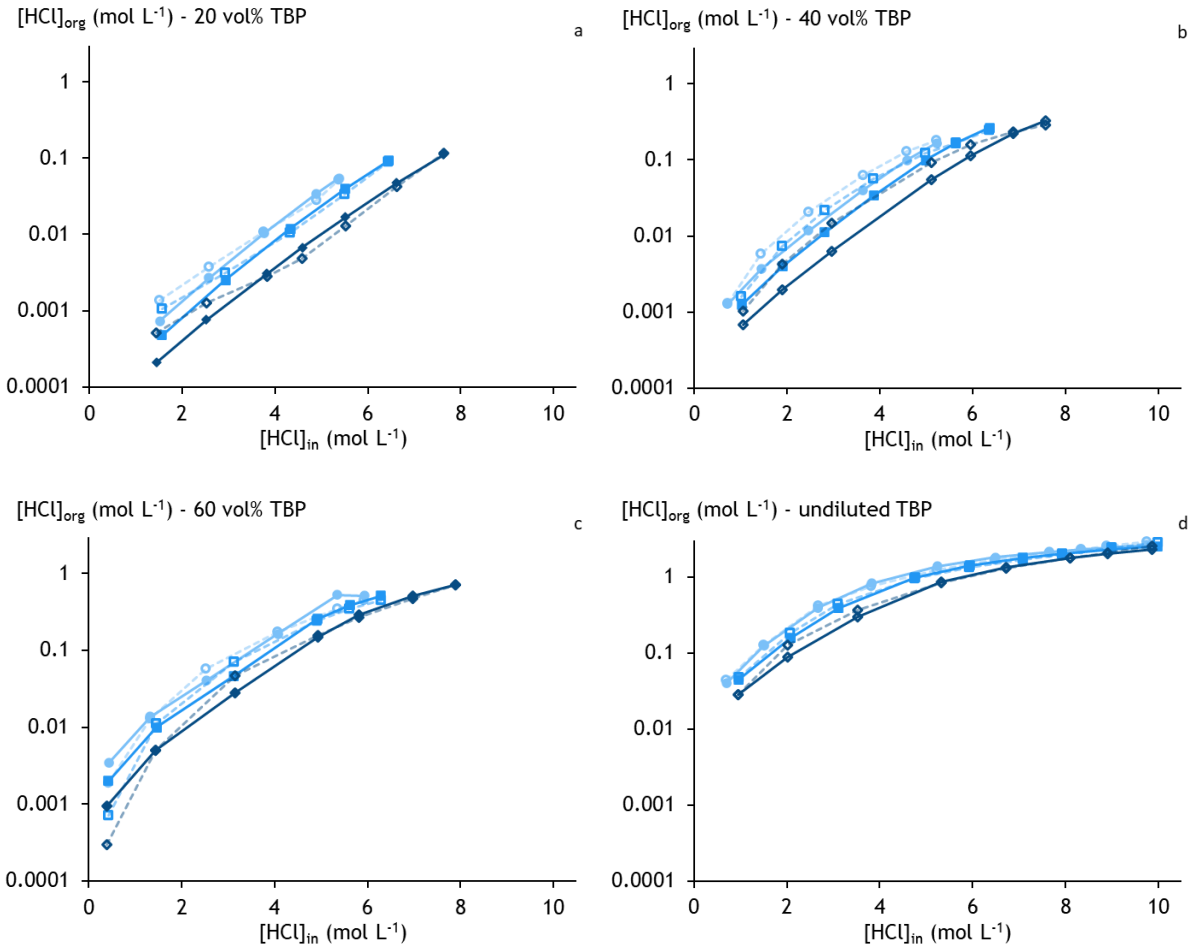

Figure 6. Model fit (filled markers) to experimental HCl extraction data (open markers) at different TBP concentrations in the organic phase (a-d) and different temperatures. Data originate from a study by Hanson and Patel, in which kerosene was used as the diluent.[49]. Temperatures: 20 °C (●), 30 °C (■), and 50 °C (◆).

4.3. Fe(III) extraction by TBP

Extraction of Fe(III) was modeled by optimizing the interaction forces between $FeCl_4^-$ and $TBP/TBPH^+$ to mimic the extraction mechanism presented in equation (5). These forces are represented in the thermodynamic model by a mid-range interaction parameter between $FeCl_4^-$ and $TBPH^+$ and short-range interaction parameters between $FeCl_4^-$ and TBP (Table 3). The OLI-MSE mid-range activity equation is typically used for ion-ion and ion-neutral species, while the OLI-MSE framework uses the UNIQUAC equation to account for the interactions between species at the short-range [33]. UNIQUAC is specifically designed to calculate phase equilibria, but it is most successful for non-electrolytes [31]. The use of UNIQUAC interaction parameters between $FeCl_4^-$ and TBP in the current thermodynamic model is justified due to the effective neutralization of the negative charge of $FeCl_4^-$ by $TBPH^+$ in the organic phase.

A temperature correction was included in the $FeCl_4^-$ – TBP UNIQUAC interaction parameters to model the extraction of Fe(III) by TBP at different temperatures:

$$a_{ij} = a_{0,ij} + a_{1,ij}T \tag{8}$$

Here, a_{ij} represents one UNIQUAC binary interaction parameter between species i and j. The UNIQUAC model has asymmetrical interaction parameters, where $a_{ij} \neq a_{ji}$ [31]. Therefore, a_{ji} also requires a temperature correction, similar to a_{ij} in equation (8). This simple linear temperature correction should suffice to model the extraction of Fe(III) within the limited range (25–55 °C) that is relevant for the solvent extraction system considered in the present study.

To avoid the extraction of the positively charged Fe^{3+}, $FeCl^{2+}$, and $FeCl_2^+$ species, repulsive mid-range interaction parameters ($b_{2,ij}$ as per equation (7)) with TBP and $TBPH^+$ were added to

the model (Table 3). This is accomplished using the same approach as used in the public OLI-MSE database for interactions between ions and molecular solvents. A fixed value of -7626.9 was chosen for these interactions, which mirrors the Fe^{3+} – *n*-dodecane mid-range interaction in the public OLI-MSE database. Similarly, the $b_{2,ij}$ for Na^+ – TBP/$TBPH^+$ was set to -7583.2 to avoid extraction of Na^+ when data with NaCl was used. This value is also present in the general OLI database for the interaction between Na^+ and *n*-dodecane.

No interaction parameters containing $FeCl_3$ were optimized. No repulsive interaction forces with $TBPH^+$ and TBP were added because $FeCl_3$ can be extracted by TBP according to the literature, while no attractive interactions were introduced either because literature data indicate that $FeCl_4^-$ is the main extracted species (*vide supra*). $FeCl_3$ can still distribute between the organic and aqueous phases in the thermodynamic model, depending on its activity in both phases. The activity in the aqueous phase is modeled based on speciation and water activity data (Figure 3 and Figure 4). In the organic phase, the absence of interaction parameters with TBP and $TBPH^+$ implies that short-range interactions between $FeCl_3$ and TBP/$TBPH^+$ are negligible compared to those between $FeCl_4^-$ and $TBPH^+$/TBP.

Furthermore, no specific interaction parameters between $FeCl_3$/$FeCl_4^-$ and *n*-dodecane were optimized, since an accurate fit of Fe(III) extraction in diluted TBP could be obtained without them. This suggests that there is no specific stabilization of the extracted Fe(III) species by *n*-dodecane in the organic phase. Of course, both TBP and $TBPH^+$ have interaction parameters with *n*-dodecane, which were determined for the inorganic acid – TBP thermodynamic model [32]. They did not require any reoptimization for the extraction of Fe(III) by TBP.

The interaction parameters between Fe(III) and other species were optimized using the aqueous data from Section 4.1 (Aqueous Fe(III) chemistry**)**, extraction data from the literature (Table 2), and new experimental data to model temperature effects. Apart from the newly introduced $FeCl_4^-$ – TBP/$TBPH^+$ parameters, these also include a reoptimization of parameters and thermodynamic values from section 4.1, and the introduction of a $FeCl_4^-$ – Cl^- mid-range interaction parameter to finetune the model.

Table 2. Overview of the Fe(III) solvent extraction data from the literature used to optimize the Fe(III) – chloride – TBP thermodynamic model. All data are collected at room temperature and with aliphatic diluents, unless otherwise stated.

Exp. number	**$[FeCl_3]_{in}$ mol L^{-1}**	**$[HCl]_{in}$ mol L^{-1}**	**$[NaCl]_{in}$ mol L^{-1}**	**$[TBP]_{org}$ mol L^{-1} (vol%)**	**O/A_{in} [a]**	**Source**
1	0.96	0.7–3.4	/	3.7 (100)	1	[43]
2	0.96	2.02	/	0-3.7 (0–100)	1	[43]
3	0.018	0.05–5.0	/	0.1/0.5 (3/14)	1	[51]
4	0.018	2.0	0.5–3.0	0.1/0.5 (3/14)	1	[51]
5	0.018	3.0 and 3.6	/	0.05-0.76 (1–20)	1	[51]
6	0.17	0.8-9.3	/	0.37 (10)	1	[8]
7	0.17	3.4–5.4	2.0-0.4	0.37 (10)	1	[8]
8	0.17	4.6 and 5.6	0-1.5	0.37 (10)	1	[8]
9	0.33	6.7	/	0.08–0.94 (2–26)	1	[8]
10	0.47	0.04–3.9 [c]	0-3.9	1.8 (50) [b]	2	[9]
11	0.47	0.1–4.0	/	1.8 (50) [b]	2	[9]
12	0.45–1.8	0.45–1.8	/	1.7 (47) [b]	1-4	[9]
13	1.8	0.27–2.7	/	0.75–3.7 (20–100) [d]	2	[41]

[a] O/A_{in} = initial organic-to-aqueous phase volume ratio
[b] 20 vol% octanol was added to the organic phase as a phase modifier
[c] This dataset also contains $HClO_4$
[d] Benzene was used as diluent

Data from the literature was used when its organic phase comprised an aliphatic diluent and no phase modifier. Due to a limited number of data points that match these requirements, data from Yi *et al*., and Sahu and Das were also used [9,41]. Yi *et al*. used 1-octanol as a phase modifier to avoid three-phase-formation, but they also showed that 1-octanol had little impact on the extraction of Fe(III). Sahu and Das also adjusted their organic phase to avoid three-phase formation. They used the aromatic diluent benzene instead of an aliphatic diluent, and the use of another diluent should slightly change the extractability of Fe(III) [52]. Nevertheless, this dataset was included because it contained valuable data over a wide range of HCl and TBP concentrations at a high Fe(III) content. The weight of the data points of Sahu and Das was lowered, so that the resulting error on the fit was comparable to that of any other dataset. This was done to avoid incorporating too much of the benzene effects in the thermodynamic model that is based on *n*-dodecane as diluent.

The new experimental data cover the extraction of Fe(III) and HCl between 25 °C and 55 °C from feed solutions with 0.1 mol L^{-1} $FeCl_3$ and 0.1 – 4.5 mol L^{-1} HCl. The organic phase consisted of 50 vol% TBP in *n*-dodecane or 100 vol% TBP. The extraction of Fe(III) does not change significantly with increasing temperature (Figure 7). This trend is less clear at the lowest and highest HCl concentrations due to an increased scatter of the data points. It is challenging to reduce this scatter at very high and very low distribution ratios *D*, because small changes in the measured aqueous metal concentration strongly affect the *D* values. In contrast to Fe(III) extraction, HCl extraction is significantly reduced at higher temperatures (Figure 8). Here, the increased scatter at low total HCl concentrations can be explained by the increased relative error on the chloride determination of samples with less HCl in the feed and equilibrium aqueous phase.

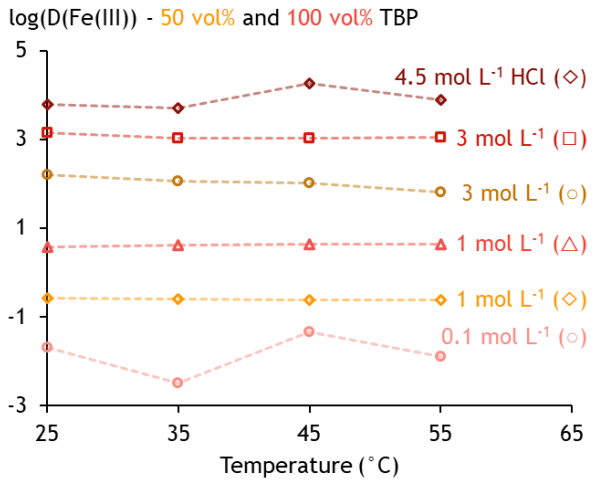

Figure 7. Experimental distribution ratio (D) of the temperature-dependent solvent extraction of Fe(III) from HCl media by 50 vol% TBP (◇, ○) in n-dodecane or 100 vol% TBP (○, △, □, ◇) at O/A of 1. 0.1 mol L^{-1} $FeCl_3$ was added to the aqueous feed.

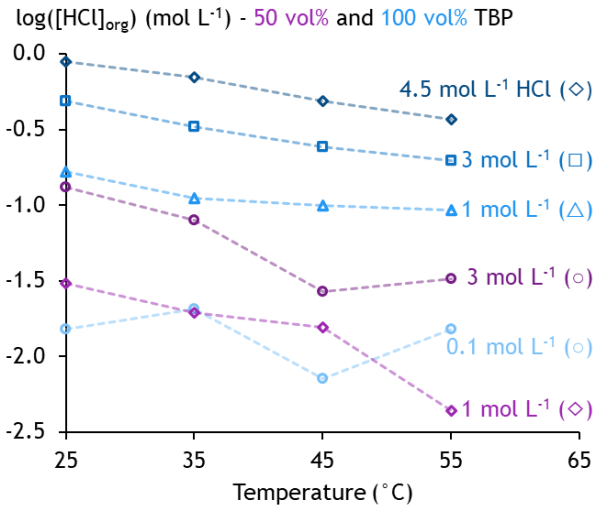

Figure 8. Experimental results of the temperature-dependent HCl extraction by 50 vol% TBP (◇, ○) in n-dodecane or 100 vol% TBP (○, △, □, ◇) at O/A of 1. 0.1 mol L^{-1} $FeCl_3$ was added to the aqueous feed.

The approach presented above allows to accurately fit the $\Delta G_{TR}(\mathrm{Fe(III)})$ values (equation (3)) of 179 data points according to an OLS analysis of the thermodynamic model fit and experimental data (Figure 9). Note that the new experiments (Figure 9, brown diamonds) are not included in the OLS analysis, because the remaining variance after OLS analysis on these points remained significantly higher than the variance on the other data sets (see Supporting Information). This significantly higher variance can be explained by the experimental difficulties in measuring very high extraction efficiencies (very low $\Delta G_{TR}(\mathrm{Fe(III)})$ in Figure 9). The Fe(III) concentration in the raffinate measured by ICP-OES was close to the quantification limit, and the resulting larger error strongly propagates to the calculation of the distribution ratio and the $\Delta G_{TR}(\mathrm{Fe(III)})$.

Some significant variance in the Fe(III) extraction data is not explained by the OLS analysis (Figure 9, $R^2 = 0.90$). Nevertheless, there is a non-significant deviation between the slope of the OLS line and that of the ideal fit line, as the OLS line falls within 2 standard deviations of the ideal slope (1). In contrast, there is a significant deviation between the intercept of the OLS line and the ideal fit line. At a 95% interval, a predicted $\Delta G_{TR}(\mathrm{Fe(III)})$ by the thermodynamic model will fall within ± 3.37 kJ mol^{-1} of a newly performed experimental value. The slight lack of fit and the rather large prediction interval show a further analysis might be useful.

A significant part of this remaining variance is most probably caused by differences between the different literature sources. This was further investigated using Restricted Maximum Likelihood (REML) analysis and Least Squares (LS) estimates. REML can then be used to verify whether there is a significant correlation between the variance of the residuals. More precisely, REML can analyze whether there is grouping in the data, and estimate how much of the remaining variance in the data is caused by that grouping. The details of this analysis can be found in the Supporting Information. REML shows that differences between different literature sources can

explain a significant portion (38%) of the remaining variance. The new LS analysis of the thermodynamic model fit versus experimental Fe(III) SX data, which includes grouping per data source, has a slope of 0.979 ± 0.024 and an intercept of 0.219 ± 0.533. The prediction interval decreases from ± 3.37 kJ mol $^{-1}$ to ± 2.78 kJ mol^{-1}. Thus, the statistical fit and the prediction interval clearly improve by accounting for the differences between different literature sources.

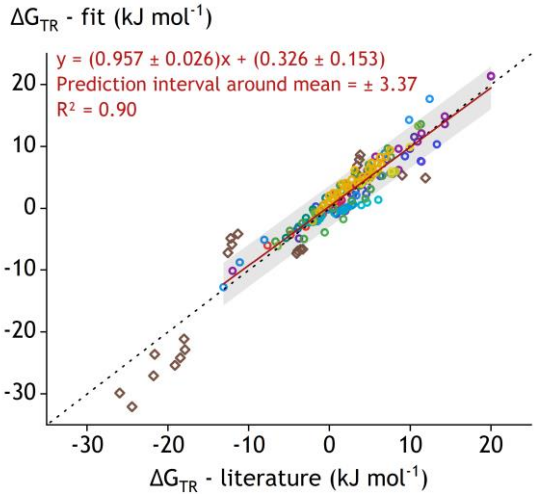

Figure 9. OLS analysis (dark red line) of thermodynamic model fit and experimental Fe(III) extraction data. Literature data are colored per experimental number, and the brown diamonds (◇) depict the new experiments. Also shown are perfect the fit line (dotted black), and the 95% prediction interval (light gray).

Note that the remaining variance on the LS analysis with source grouping can come from the thermodynamic model and/or experimental errors within datasets. It is still not possible to determine the prediction error on the thermodynamic model alone, based on the fitted data. Therefore, a separate validation of the whole thermodynamic model is performed by predicting other experimental data, focused on the extraction of Fe(III) (*vide infra*). Furthermore, the individual fit plots of the actual data can be found in the Supporting Information.

There are some limitations to the use of the Fe(III) – chloride – TBP thermodynamic model that are inherent to the OLI-MSE framework when applied to solvent extraction systems. TBP, highly loaded with HCl and/or $FeCl_4^-$, is not soluble anymore in aliphatic diluents. For instance, this led to third-phase formation in a system with 30 vol% TBP in *n*-octane above 7.6 mol L^{-1} HCl in the aqueous phase [53]. Thermodynamic models created with the OLI-MSE framework cannot predict this third-phase formation, as the OLI-MSE framework cannot take more than two liquid phases into account.

Furthermore, extractants have surfactant-like properties that might result in the formation of reverse micelles and microemulsions in the organic phase. These phenomena cannot be treated using the OLI-MSE framework [54]. Both the ability to construct an accurate model and the literature suggest that this supramolecular organization of the organic phase does not occur for most conditions used to construct the thermodynamic model. Reverse micelles are expected at conditions close to the ones where a third phase is formed [53,55]. Hence, the presented thermodynamic model will perform worse close to this limit of third-phase formation.

Table 3. Optimized short- and mid-range binary interaction parameters in the Fe(III) – chloride – TBP thermodynamic model.

Species	Short-range [a]		Mid-range [b]	
	a_{ij}	a_{ji}	b_{ij}	c_{ij}
Fe^{3+} – H_2O			18.987	
$FeCl^{2+}$ – H_2O			14.490	
$FeCl_2^+$ – H_2O			20.037	
$FeCl_3$ – H_2O			20.772	
$FeCl_4^-$ – H_2O			13.537	
$FeCl_4^-$ – Cl^-			-6.3259	
TBP – HCl (0) [c]	0		0.14163 [d]	-16.767 [d]
TBP – HCl (2) [c]				7624.4 [d]
$TBPH^+$ – HCl			8.1072	
TBP – Cl^-			-6.5913	
$TBPH^+$ – Cl^-			-17.211	15.412 [d]
n-dodecane – HCl (0)			-15.202 [d]	-0.17061 [d]
n-dodecane – HCl (2)			5344.9 [d]	
n-dodecane – Cl^- (2)			-9069.5 [d]	3688.2 [d]
$FeCl_4^-$ – TBP (0) [e]	-701.14	-3030.4		
$FeCl_4^-$ – TBP (1) [e]	-20.354	-20.354		
$FeCl_4^-$ – $TBPH^+$			-0.3896	
$FeCl_4^-$ – *n*-dodecane				0 [f]
$FeCl_x^{3-x}$ (x = 0–2) – TBP (2) [c]				-7626.9
$FeCl_x^{3-x}$ (x = 0–2) – $TBPH^+$ (2) [c]				-7626.9
Na^+ – TBP (2) [c]				-7583.2
Na^+ – $TBPH^+$ (2) [c]				-7583.2

[a] Short-range binary interaction parameters.

[b] Mid-range binary interaction parameters: b_{ij} and c_{ij} according to equation (7).

[c] (0) = $b_{0,ij}$ and $c_{0,ij}$; (2) = $b_{2,ij}$ and $c_{2,ij}$ according to equation (7).

[d] Unchanged value from the acid – TBP thermodynamic model [32].

[e] (0) = $a_{0,ij}$ or $a_{0,ji}$; (1) = $a_{1,ij}$ or $a_{1,ji}$ according to equation (8).

[f] Changed value compared to the public OLI-MSE database.

3.3. Model validation

The final thermodynamic model was validated to verify its predictive capabilities by comparing calculations and experimental data from systems that have not been used to build the model. Ideally, these systems have compositions that are significantly different from the systems that have been used in the fitting procedure, to verify whether the model can make extrapolations.

First, the extraction of Fe(III) from sulfate media was calculated based on data from Qifeng *et al*. [11]. They used two feed solutions of Fe(III) in sulfuric acid and found a distribution ratio of less than 0.01 for the extraction of Fe(III) by TBP. The first feed contained 0.56 mol L^{-1} Fe(III) in 3.1 mol L^{-1} H_2SO_4 and the second consisted of 0.05 mol L^{-1} Fe(III) at a pH of 0.64. The equilibrium after contacting these feeds with 10 – 100 vol% TBP in *n*-dodecane was calculated with the thermodynamic model and no significant extraction of Fe(III) was found, matching with the experimental data. These findings can be explained by the very limited sulfate complexation to Fe(III), leading to virtually no neutral or anionic Fe(III) complexes. Note that the aqueous sulfate chemistry of Fe(III) is present in the public OLI-MSE database and the extraction of H_2SO_4 (with protonation of TBP) is present due to the use of the inorganic acid – TBP database [32].

Next, the thermodynamic model was validated with more complex chloride solutions that contained significant quantities of other metal ions next to Fe(III). Only a limited number of literature sources could be found that matched these criteria, which all used a modifier or an aromatic diluent to improve the phase behavior. Eventually, two systems described in the literature were used [10,56]. The details of these systems can be found in Table 4. A new experiment that uses no (aromatic) diluent or modifier is also included in the table. This allowed verifying the predictive capacities of the thermodynamic model without any additional compounds that might

influence the extraction beyond the scope of the constructed model. The experiment was performed following the same method as explained in Section 2.1.

Table 4. Overview of the validation data from the literature and a new experiment (n.e.) in chloride media. All data are recorded at room temperature.

Exp. No.	$[Fe(III)]_{in}$ mol L^{-1}	$[M]_{in}$ [a] mol L^{-1}	$[HCl]_{in}$ mol L^{-1}	$[H_2SO_4]_{in}$ mol L^{-1}	$[TBP]_{org}$ mol L^{-1}	Diluent	O/A_{in}	Reference
1	0.211	1.06 [c]	4.97	0.51	0.5–2.5	Kerosene [d]	1	[10]
2	0.211	1.06 [c]	4.97	0.51	1.73	Kerosene [d]	0.2 – 5	[10]
3	0.29	0.55 [e]	4.3–8.6	/	1.8	Benzene	1	[56]
4	0.29	0.55 [e]	2.4–7.6	/	0.92	Benzene	1	[56]
5	0.29	0.29 [e]	1.7–8.4	/	0.92	Benzene	1	[56]
6	0.29	0.17 [f]	5.55	/	3.65	None	1	n.e.

[a] Total concentration of other metals (not Fe(III)) in the feed
[b] O/A_{in} = initial organic to aqueous phase volume ratio
[c] M = Cu(II), Zn(II), Co(II), and Ni(II)
[d] 20 vol% methyl isobutyl ketone added as a modifier
[e] M = Ti(IV)
[f] M = Cu(II), Zn(II), Co(II), Ni(II), Mn(II), Mg(II), and Ca(II)

To avoid an incorrect prediction of coextraction of the other metals in the feed, repulsive binary interaction parameters were added between the most abundant cationic species of these metals and TBP/$TBPH^+$, following the same approach as for the cationic Fe(III) species (*vide supra*). More precisely, a $b_{2,ij}$ value of -7626.9 was added to the model for these interactions.

The first set of chloride media validation data contained 20 vol% methyl isobutyl ketone (MIBK) as a modifier. This significantly impacted the extraction of Fe(III) as MIBK also extracts Fe(III) [43]. To compensate for the addition of the modifier in the experimental data, it was

replaced by the 20 vol% TBP in the calculation. After this, an acceptable prediction of both the TBP dependence on Fe(III) extraction and the Fe(III) extraction isotherm of Sarangi *et al*. were obtained (Figure 10). These are experimental numbers 1 and 2 in Table 4. Also shown in Figure 10 (a) is the prediction and experimental data for Zn(II) extraction. This element from the feed is the second-most efficiently extracted by TBP after Fe(III). Both the prediction and experiment show no significant Zn extraction.

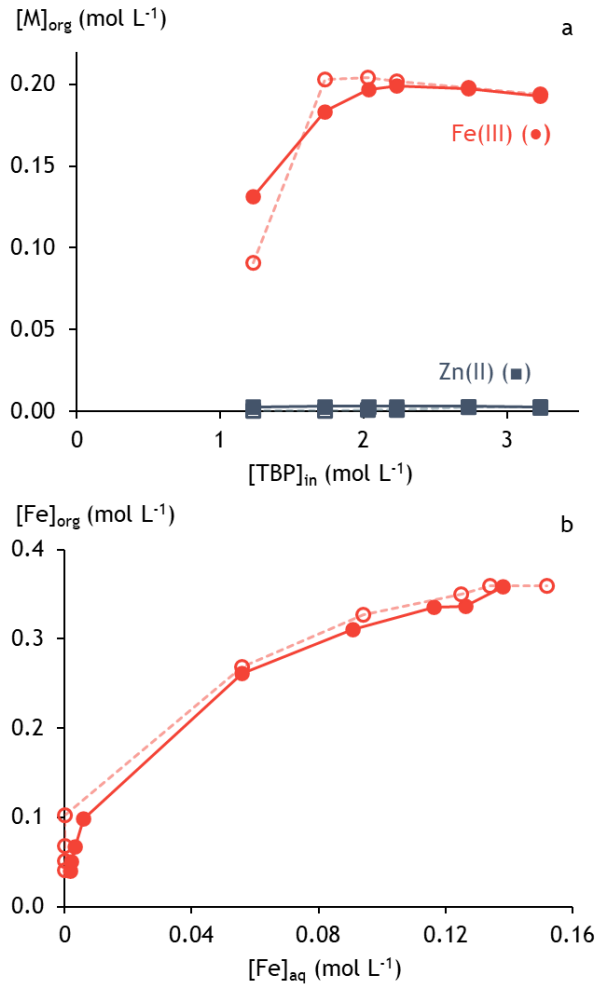

Figure 10. Model prediction (filled markers) to experimental extraction data (open markers) at different TBP concentrations in the organic phase (a) and different volume ratios (b). Data originate from Sarangi et al. [10].

The second set of validation data in chloride media is from Narita *et al*. and deals with mixed Fe(III)–Ti(IV) feeds for the production of pure Ti(IV) from ilmenite ore [56]. Fe(III) is preferentially extracted at low chloride concentrations, but Ti(IV) starts to be coextracted significantly above 8 mol L^{-1} HCl. The thermodynamic model is only designed to calculate the extraction of Fe(III). Thus, only data without significant coextraction of Ti(IV) are used for the validation because the model cannot predict loading effects due to the extraction of Ti(IV). Unfortunately, these data are produced with an organic phase that contains an aromatic diluent, which results in a slightly underestimated Fe(III) extraction by the prediction (Figure 11).

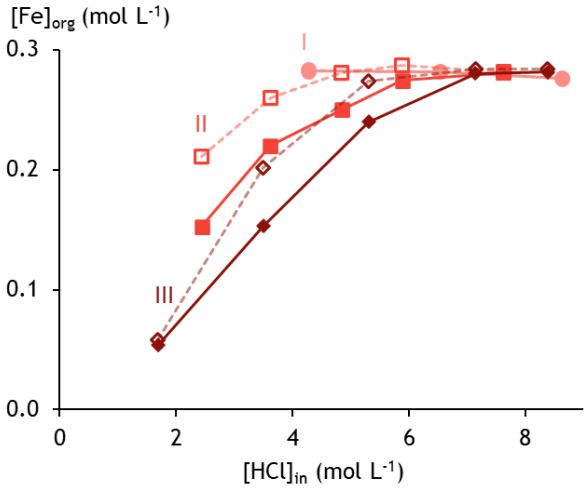

Figure 11. Model prediction (filled markers) to experimental extraction data (open markers) from Narita et al. [56]. Experimental conditions: I = Table 4 (No. 3), II = Table 4 (No. 4), and III = Table 4 (No. 5).

The last set of validation data in chloride medium is a single new experiment (Table 4, No. 6). The prediction and the experimental results both show an extraction percentage of Fe(III) above 99.9% and they give an HCl extraction of 11.6% (predicted) and 11.7% (experimental). The validation of HCl extraction is relevant because the thermodynamic model contains that chemistry.

From all metal ions present in the feed, Zn(II) and Cu(II) are the only elements coextracted with Fe(III). Still, their low concentrations in the feed (0.0046 mol L^{-1} and 0.0063 mol L^{-1} respectively) do not lead to any loading effects on the extraction of Fe(III). These elements are coextracted because chloride anions coordinate to them at the chloride concentration used in the experiment [57,58]. The experimentally observed percentage extraction was 73% for Zn(II) and 15% for Cu(II). The chemistry of Zn(II) and Cu(II) extraction is not optimized in the model, except for the repulsive interaction between their most abundant cations in chloride media and TBP/$TBPH^+$ (*vide supra*). An accurate prediction of Zn(II) and Cu(II) extraction is not expected. Nevertheless, Zn(II) is 92% extracted due to the migration of $ZnCl_4^{2-}$ to the organic phase. Cu(II) is not extracted according to the model. Charge neutrality in the organic phase is probably maintained by $TBPH^+$ for $ZnCl_4^{2-}$.

The overall agreement between a predicted Fe(III) extraction by the thermodynamic model and its corresponding experimental value in (mixed) chloride systems (Table 4) can be assessed by an OLS analysis of the predicted $[Fe(III)]_{org}$ versus its experimental value (Figure 12). There is a non-significant deviation between the OLS line and the ideal statistical fit line, but the prediction interval still allows for a certain deviation between a new prediction by the thermodynamic model of a newly measured experimental Fe(III) extraction value. The width of this prediction interval is the result of both unexplained physicochemical processes and contributions in the thermodynamic model, and errors on the experimental measurements. Overall, the predictions by the thermodynamic model match quite well with the experimental data, certainly considering a modifier or an aromatic diluent was used in the two literature sources. This modifier and aromatic diluent are most likely part of the unexplained physicochemical processes and contributions in the

thermodynamic model, as they were not included during the construction of the thermodynamic model.

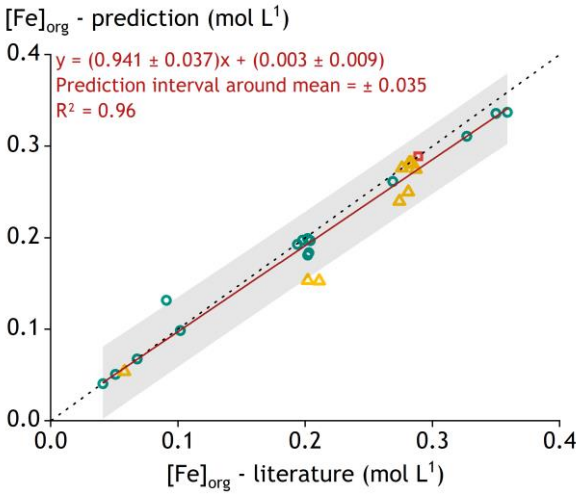

Figure 12. OLS analysis (dark red line) of thermodynamic model prediction and experimental Fe(III) extraction data. Different colored data points are from different datasets: new experiment (□), Sarangi et al. [10] (○), and Narita et al. [56] (△). The black dotted line represents a perfect fit, and the prediction interval is shown in light gray

Finally, the temperature-dependent data that were used to optimize the extraction of Fe(III) (Figure 7) also contain data on the extraction of HCl (Figure 8). The latter data were not used to optimize any interaction parameters or other thermodynamic values for the extraction of HCl. They can be used to validate the extraction of HCl in the presence of Fe(III). These data are valuable to test the predictive qualities of the model because the extraction of HCl was not optimized in systems with coextraction of metals. The prediction of the HCl extraction by undiluted TBP is very good (Figure 13), considering there is significant scatter on the experimental data at the lowest initial HCl concentration. The prediction of the HCl extraction by 50 vol% TBP shows a larger deviation, but this can (partially) be explained by a larger scatter of the experimental data due to

the challenges related to an accurate determination of a low HCl extraction based on the HCl content in the feed and aqueous phase at equilibrium.

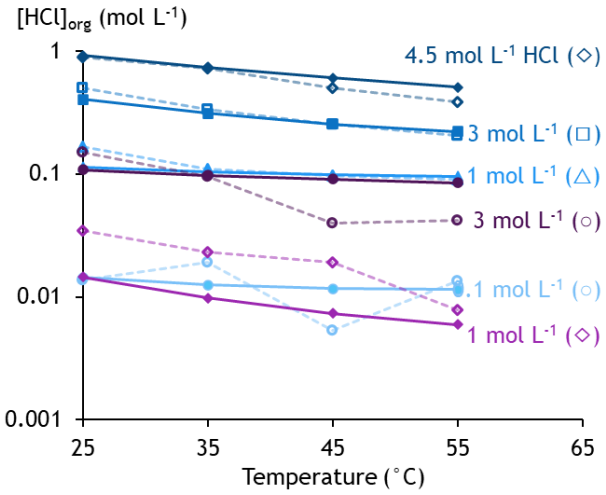

Figure 13. Predicted (filled markers) and experimental results (open markers) of the temperature-dependent HCl extraction by 50 vol% TBP (◇, ○) in n-dodecane or 100 vol% TBP (○, △, □, ◇) at O/A of 1. 0.1 mol L^{-1} $FeCl_3$ was added to the feed.

5. CONCLUSIONS

A predictive thermodynamic model for the Fe(III) – chloride – TBP system was developed to assist with the calculation of solvent extraction processes for the removal of iron from aqueous HCl solutions. This model is based on the OLI-MSE semi-empirical thermodynamic framework. The included chemical model incorporates all relevant species and interactions without adding too many (possibly fictitious) species. The chemistry consists of the coordination of chloride anions to Fe(III) in the aqueous phase, the extraction of HCl with protonation of the TBP extractant, and the stabilization of Fe(III) in the organic phase as an $[FeCl_4^-][TBPH^+][TBP]$ ion pair formed by weak interactions. This approach considers the thermodynamic non-ideality of both the aqueous and organic phase, allowing it to work in a broad range of compositions, including high metal loading of the organic phase. The final model can calculate the equilibrium of systems containing between 0% and 100% TBP in the organic phase, and it can predict the extraction of Fe(III) from complex chloride and/or sulfate aqueous feed solutions.

Author Contributions

Rayco Lommelen: Conceptualization, Methodology, Experimental Design, Validation, Formal analysis, Investigation, Validation, Writing - Original Draft, Visualization

Brecht Dewulf: Experimental Design and Work

Jakob Bussé: Experimental Work

Koen Binnemans: Conceptualization, Writing - Review & Editing, Supervision, Resources, Funding acquisition

Acknowledgments

This work was supported by the European Union's Framework Programme for Research and Innovation Horizon Europe [Grant number 101058124 (ENICON)]. We thank Dr. Tim Balcaen (KU Leuven) for his valuable help and insights when performing the statistical analysis on the agreement between the thermodynamic model and the experimental data.

Notes

The authors declare no competing financial interest.

Supporting Information

Includes the statistical correlation analysis between $FeCl^{2+}$ and $FeCl_2^+$ speciation, the advanced statistical analysis of model and experimental Fe(III) extraction data, the validation and update of the HNO_3 and H_2SO_4 extraction model due to the update of $S^0(TBPH^+)$, and the individual data fit plots for the construction of the Fe(III) extraction model.

5. REFERENCES

[1] A.J. Monhemius, The Iron Elephant: A Brief History of Hydrometallurgists' Struggles with Element No. 26., in: XXVIII International Mineral Processing Congress, Quebec City, PQ, Canada, 2016. https://doi.org/10.15834/cimj.2017.21.

[2] K. Binnemans, P.T. Jones, The Twelve Principles of Circular Hydrometallurgy, Journal of Sustainable Metallurgy 9 (2022) 1–25. https://doi.org/10.1007/s40831-022-00636-3.

[3] Z. Liu, H. Li, Metallurgical process for valuable elements recovery from red mud—A review, Hydrometallurgy 155 (2015) 29–43. https://doi.org/10.1016/j.hydromet.2015.03.018.

[4] L. Hoeber, S. Steinlechner, A comprehensive review of processing strategies for iron precipitation residues from zinc hydrometallurgy, Clean. Eng. Technol. 4 (2021) 100214. https://doi.org/10.1016/j.clet.2021.100214.

[5] K. Wang, J. Li, R.G. McDonald, R.E. Browner, Iron, aluminium and chromium co-removal from atmospheric nickel laterite leach solutions, Miner. Eng. 116 (2018) 35–45. https://doi.org/10.1016/j.mineng.2017.10.019.

[6] Y. Chang, X. Zhai, B. Li, Y. Fu, Removal of iron from acidic leach liquor of lateritic nickel ore by goethite precipitate, Hydrometallurgy 101 (2010) 84–87. https://doi.org/10.1016/j.hydromet.2009.11.014.

[7] A. Habib, H.N. Bhatti, M. Iqbal, Metallurgical Processing Strategies for Metals Recovery from Industrial Slags, Z. Phys. Chem. 234 (2020) 201–231. https://doi.org/10.1515/zpch-2019-0001.

[8] R.K. Mishra, P.C. Rout, K. Sarangi, K.C. Nathsarma, A comparative study on extraction of Fe(III) from chloride leach liquor using TBP, Cyanex 921 and Cyanex 923, Hydrometallurgy 104 (2010) 298–303. https://doi.org/10.1016/j.hydromet.2010.07.003.

[9] X. Yi, G. Huo, W. Tang, Removal of Fe(III) from Ni-Co-Fe chloride solutions using solvent extraction with TBP, Hydrometallurgy 192 (2020) 105265. https://doi.org/10.1016/j.hydromet.2020.105265.

[10] K. Sarangi, P.K. Parhi, E. Padhan, A.K. Palai, K.C. Nathsarma, K.H. Park, Separation of iron(III), copper(II) and zinc(II) from a mixed sulphate/chloride solution using TBP, LIX 84I and Cyanex 923, Sep. Purif. Technol. 55 (2007) 44–49. https://doi.org/10.1016/j.seppur.2006.10.021.

[11] Q. Wei, X. Ren, J. Guo, Y. Chen, Recovery and separation of sulfuric acid and iron from dilute acidic sulfate effluent and waste sulfuric acid by solvent extraction and stripping, J. Hazard. Mater. 304 (2016) 1–9. https://doi.org/10.1016/j.jhazmat.2015.10.049.

[12] S.I. El Dessouky, Y.A. El-Nadi, I.M. Ahmed, E.A. Saad, J.A. Daoud, Solvent extraction separation of Zn(II), Fe(II), Fe(III) and Cd(II) using tributylphosphate and CYANEX 921 in kerosene from chloride medium, Chem. Eng. Process. 47 (2008) 177–183. https://doi.org/10.1016/j.cep.2007.03.002.

[13] S. Dash, S. Mohanty, Mathematical Modeling Aspect in Solvent Extraction of Metals, Sep. Purif. Rev. 50 (2021) 74–95. https://doi.org/10.1080/15422119.2019.1648294.

[14] L. Cohen, T. McCallum, O. Tinkler, W. Szolga, Technological Advances, Challenges and Opportunities in Solvent Extraction from Energy Storage Applications, in: Extraction 2018: The Minerals, Metals & Materials Series, 2018: pp. 2033–2045. https://doi.org/10.1007/978-3-319-95022-8_170.

[15] Redbook Mining Solutions, n.d. http://www.mining-solutions.basf.com/.

[16] J. Bisson, B. Dinh, P. Huron, C. Huel, PAREX, A Numerical Code in the Service of La Hague Plant Operations, Procedia Chem. 21 (2016) 117–124. https://doi.org/10.1016/j.proche.2016.10.017.
[17] E.A. Puzikov, B.Ya. Zilberman, A.S. Kudinov, N.D. Goletskii, Description of the Extraction of Trivalent REE and TPE Nitrates with Tributyl Phosphate and Its Solutions in Paraffins in the Presence of Nitric Acid and Salting-out Agents Using a Unified Model, Radiochemistry 61 (2019) 689–693. https://doi.org/10.1134/S1066362219060080.
[18] A. Chagnes, Simulation of Solvent Extraction Flowsheets by a Global Model Combining Physicochemical and Engineering Approaches—Application to Cobalt(II) Extraction by D2EHPA, Solvent Extr. Ion Exch. 38 (2020) 3–13. https://doi.org/10.1080/07366299.2019.1691135.
[19] H. Chen, A.J. Masters, R. Taylor, M. Jobson, D. Woodhead, Application of SAFT-VRE in the Flowsheet Simulation of an Advanced PUREX Process, Ind. Eng. Chem. Res. 58 (2019) 3822–3831. https://doi.org/10.1021/acs.iecr.8b05606.
[20] C.O. Iloeje, C.F.J. Colón, J. Cresko, D.J. Graziano, Gibbs Energy Minimization Model for Solvent Extraction with Application to Rare-Earths Recovery, Environ. Sci. Technol. 53 (2019) 7736–7745. https://doi.org/10.1021/acs.est.9b01718.
[21] F. Vasilyev, S. Virolainen, T. Sainio, Modeling the liquid–liquid extraction equilibrium of iron (III) with hydroxyoxime extractant and equilibrium-based simulation of counter-current copper extraction circuits, Chem. Eng. Sci. 175 (2018) 267–277. https://doi.org/10.1016/j.ces.2017.10.003.
[22] A. Chandra, Thermodynamic Modeling and Equilibrium System Design of a Solvent Extraction Process for Dilute Rare Earth Solutions, Doctoral Dissertation, University of Kentucky, 2019. https://doi.org/10.13023/etd.2020.004.
[23] C.F.Jr. Baes, Modeling Solvent Extraction Systems with SXFIT, Solvent Extr. Ion Exch. 19 (2001) 193–213. https://doi.org/10.1081/SEI-100102691.
[24] T.H. Ibrahim, An Overview of the Physiochemical Nature of Metal-Extractant Species in Organic Solvent/Acidic Organophosphorus Extraction Systems, Sep. Sci. Technol. 46 (2011) 2157–2166. https://doi.org/10.1080/01496395.2011.594478.
[25] T. Zemb, C. Bauer, P. Bauduin, L. Belloni, C. Déjugnat, O. Diat, V. Dubois, J.-F. Dufrêche, S. Dourdain, M. Duvail, C. Larpent, F. Testard, S. Pellet-Rostaing, Recycling metals by controlled transfer of ionic species between complex fluids: en route to “ienaics,” Colloid Polym. Sci. 293 (2015) 1–22. https://doi.org/10.1007/s00396-014-3447-x.
[26] M. Špadina, K. Bohinc, T. Zemb, J.-F. Dufrêche, Multicomponent Model for the Prediction of Nuclear Waste/Rare-Earth Extraction Processes, Langmuir 34 (2018) 10434–10447. https://doi.org/10.1021/acs.langmuir.8b01759.
[27] M. Špadina, K. Bohinc, T. Zemb, J.-F. Dufrêche, Colloidal Model for the Prediction of the Extraction of Rare Earths Assisted by the Acidic Extractant, Langmuir 35 (2019) 3215–3230. https://doi.org/10.1021/acs.langmuir.8b03846.
[28] S. Gourdin-Bertin, J.-F. Dufrêche, M. Duvail, T. Zemb, Microemulsion as Model to Predict Free Energy of Transfer of Electrolyte in Solvent Extraction, Solvent Extr. Ion Exch. 40 (2022) 28–63. https://doi.org/10.1080/07366299.2021.1953259.
[29] F. Eckert, M. Diedenhofen, A. Klamt, Towards a first principles prediction of pK a: COSMO-RS and the cluster-continuum approach, Mol. Phys. 108 (2010) 229–241. https://doi.org/10.1080/00268970903313667.

[30] B. Zhuang, G. Ramanauskaite, Z.Y. Koa, Z.-G. Wang, Like dissolves like: A first-principles theory for predicting liquid miscibility and mixture dielectric constant, Sci. Adv. 7 (2021). https://doi.org/10.1126/sciadv.abe7275.
[31] J. Prausnitz, R. Lichtenthaler, E.G. de Azevedo, Molecular Thermodynamics of Fluid-Phase Equilibria, 3rd Edition, Pearson, Upper Saddle River NJ, Upper Saddle River, N.J, 1998.
[32] R. Lommelen, K. Binnemans, Molecular thermodynamic model for solvent extraction of mineral acids by tri-n-butyl phosphate (TBP), Sep. Purif. Technol. 313 (2023) 123475. https://doi.org/10.1016/j.seppur.2023.123475.
[33] P. Wang, A. Anderko, R.D. Young, A speciation-based model for mixed-solvent electrolyte systems, Fluid Phase Equilib. 203 (2002) 141–176. https://doi.org/10.1016/S0378-3812(02)00178-4.
[34] P. Wang, A. Anderko, R.D. Springer, R.D. Young, Modeling phase equilibria and speciation in mixed-solvent electrolyte systems: II. Liquid–liquid equilibria and properties of associating electrolyte solutions, J. Mol. Liq. 125 (2006) 37–44. https://doi.org/10.1016/j.molliq.2005.11.030.
[35] Leslie Miller, AJ Gerbino, HEHEHP Database to Predict Rare Earth Solvent Extraction, in: ALTA 2023 Uranium-Rare Earths Conference, Perth, Australia, 30 April - 6 May 2023.
[36] J. Rydberg, M. Cox, C. Musikas, G.R. Choppin, Solvent Extraction Principles and Practice, Revised and Expanded, 2nd ed., Marcel Dekker, New York, New York, 2004.
[37] J. Narbutt, Chapter 4 - Fundamentals of Solvent Extraction of Metal Ions, in: C.F. Poole (Ed.), Liquid-Phase Extraction, Elsevier, Amsterdam, 2020: pp. 121–155. https://doi.org/10.1016/B978-0-12-816911-7.00004-9.
[38] S.K. Majumdar, A.K. De, Liquid-liquid extraction of iron(III) with tributylphosphate: Separation from mixtures, Talanta 7 (1960) 1–6. https://doi.org/10.1016/0039-9140(60)80002-1.
[39] M.-S. Lee, G.-S. Lee, K.Y. Sohn, Solvent Extraction Equilibria of $FeCl_3$ with TBP, Mater. Trans. 45 (2004) 1859–1863. https://doi.org/10.2320/matertrans.45.1859.
[40] W. Liu, B. Etschmann, J. Brugger, L. Spiccia, G. Foran, B. McInnes, UV–Vis spectrophotometric and XAFS studies of ferric chloride complexes in hyper-saline LiCl solutions at 25–90 °C, Chem. Geol. 231 (2006) 326–349. https://doi.org/10.1016/j.chemgeo.2006.02.005.
[41] K.K. Sahu, R.P. Das, Synergistic extraction of iron(III) at higher concentrations in D2EHPA-TBP mixed solvent systems, Metall. Mater. Trans. B 28 (1997) 181–189. https://doi.org/10.1007/s11663-997-0083-6.
[42] A. Zhao, T. Zhang, Study on Extraction and Separation Performance of Iron and Aluminum from Acid Leaching Solution of High-Iron Bauxite, Russ. J. Non-Ferr. Met. 63 (2022) 37–45. https://doi.org/10.3103/S1067821222010023.
[43] B.R. Reddy, P.V.R. Bhaskara Sarma, Extraction of iron(III) at macro-level concentrations using TBP, MIBK and their mixtures, Hydrometallurgy 43 (1996) 299–306. https://doi.org/10.1016/0304-386X(95)00117-Y.
[44] H. Su, Z. Li, Z. Zhu, L. Wang, T. Qi, Extraction relationship of Li^+ and H^+ using tributyl phosphate in the presence of Fe(III), Sep. Sci. Technol. 55 (2020) 1677–1685. https://doi.org/10.1080/01496395.2019.1604759.

[45] Y. Awakura, Y. Kawasaki, A. Uno, K. Sato, H. Majima, Activities of water and HCl in Aqueous solution systems of HCl MCl_n including $CuCl_2$, $NiCl_2$ and $FeCl_3$, Hydrometallurgy 19 (1987) 137–157. https://doi.org/10.1016/0304-386X(87)90001-6.
[46] A.V. Rumyantsev, S. Hagemann, H.C. Moog, Isopiestic Investigation of the Systems $Fe_2(SO_4)_3$–H_2SO_4–H_2O, $FeCl_3$–H_2O, and Fe(III)–(Na, K, Mg, Ca)Cl_n–H_2O at 298.15 K, Z. Phys. Chem. 218 (2004) 1089–1127. https://doi.org/10.1524/zpch.218.9.1089.41670.
[47] A.S. Kertes, Solute-solvent interaction in the system hydrochloric acid-water-tri-n-butyl phosphate, J. Inorg. Nucl. Chem. 14 (1960) 104–113. https://doi.org/10.1016/0022-1902(60)80206-0.
[48] E. Hesford, H.A.C. McKay, The extraction of mineral acids by tri-n-butyl phosphate (TBP), J. Inorg. Nucl. Chem. 13 (1960) 156–164. https://doi.org/10.1016/0022-1902(60)80248-5.
[49] C. Hanson, A.N. Patel, Distribution of hydrochloric acid between tri-n-butyl phosphate and water, J. Appl. Chem. 18 (1968) 209–212. https://doi.org/10.1002/jctb.5010180705.
[50] P. Wang, R.D. Springer, A. Anderko, R.D. Young, Modeling phase equilibria and speciation in mixed-solvent electrolyte systems, Fluid Phase Equilib. 222–223 (2004) 11–17. https://doi.org/10.1016/j.fluid.2004.06.008.
[51] N. Sadeghi, E.K. Alamdari, Separation of Fe(III) from chloride solution by solvent extraction method and Tri-n-butyl phosphate (TBP), in: 20th International Solvent Extraction Conference, Würzburg Germany, 2014.
[52] M. Regadío, N.K. Batchu, K. Binnemans, Selection criteria of diluents of tri-n-butyl phosphate for recovering neodymium(III) from nitrate solutions, Chem. Eng. Res. Des. 161 (2020) 304–311. https://doi.org/10.1016/j.cherd.2020.07.016.
[53] R. Chiarizia, P.G. Rickert, D. Stepinski, P. Thiyagarajan, K.C. Littrell, SANS Study of Third Phase Formation in the HCl-TBP-n-Octane System, Solvent Extr. Ion Exch. 24 (2006) 125–148. https://doi.org/10.1080/07366290500464300.
[54] R. Lommelen, K. Binnemans, Thermodynamic Modeling of Salting Effects in Solvent Extraction of Cobalt(II) from Chloride Media by the Basic Extractant Methyltrioctylammonium Chloride, ACS Omega 6 (2021) 11355–11366. https://doi.org/10.1021/acsomega.1c00340.
[55] J. Jiang, W. Li, H. Gao, J. Wu, Extraction of inorganic acids with neutral phosphorus extractants based on a reverse micelle/microemulsion mechanism, J. Colloid Interface Sci. 268 (2003) 208–214. https://doi.org/10.1016/j.jcis.2003.08.045.
[56] E. Narita, H. Takeuchi, H. Ichikawa, T. Odagawa, T. Okabe, Manufacture of Pure Titanium(IV) Oxide by the Chloride Process. II. Selective Extraction of Titanium(IV) and Iron(III) from Hydrochloric Acid Leach Liquor of Ilmenite Ore by Tributyl Phosphate, Bull. Chem. Soc. Jpn. 56 (1983) 1832–1836. https://doi.org/10.1246/bcsj.56.1832.
[57] R. Lommelen, T. Vander Hoogerstraete, B. Onghena, I. Billard, K. Binnemans, Model for Metal Extraction from Chloride Media with Basic Extractants: A Coordination Chemistry Approach, Inorg. Chem. 58 (2019) 12289–12301. https://doi.org/10.1021/acs.inorgchem.9b01782.
[58] R. Lommelen, K. Binnemans, Hard–Soft Interactions in Solvent Extraction with Basic Extractants: Comparing Zinc and Cadmium Halides, ACS Omega 6 (2021) 27924–27935. https://doi.org/10.1021/acsomega.1c03790.